Original Article

MOLECULAR METABOLISM

Proteomic quantitative study of dorsal root ganglia and sciatic nerve in type 2 diabetic mice

Marc Leal-Julià [1,2,6], Jorge J. Vilches [1,3], Andrea Onieva [1,2,6], Sergi Verdés [1,2,6], Ángela Sánchez [1,2,6], Miguel Chillón [1,2,4,6], Xavier Navarro [1,3,5], Assumpció Bosch [1,2,5,6,*]

ABSTRACT

Objective: Peripheral neuropathy is the most common and debilitating complication of type 2 diabetes, leading to sensory loss, dysautonomia, hyperalgesia, and spontaneous noxious sensations. Despite the clinical and economic burden of diabetic neuropathy, no effective treatment is available. More preclinical research must be conducted in order to gain further understanding of the aetiology of the disease and elucidate new therapeutic targets.

Methods: The proteome of lumbar dorsal root ganglia and sciatic nerve of BKS-*db/db* mice, which contain a mutation of the leptin receptor and are an established type 2 diabetes model, was characterized for the first time by tandem mass tag labelling and mass spectrometry analysis.

Results: Proteomic analysis showed differentially expressed proteins grouped into functional clusters in *db/db* peripheral nerves compared to control mice, underlining reduced glycolytic and TCA cycle metabolism, higher lipid catabolism, upregulation of muscle-like proteins in DRG and downregulation in SCN, increased cytoskeleton-related proteins, a mild dysregulation of folding chaperones, activation of acute-phase and inflammatory response, and alterations in glutathione metabolism and oxidative stress related proteins.

Conclusions: Our data validate previous transcriptomic and metabolomic results and uncover new pathways altered in diabetic neuropathy. Our results point out that energetic deficiency could represent the main mechanism of neurodegeneration observed in diabetic neuropathy. These findings may provide important information to select appropriate targets to develop new therapeutic strategies.

Keywords Diabetes; Obesity; Neuropathy; Proteomics; Dorsal root ganglia; Sciatic nerve

1. INTRODUCTION

Diabetic complications represent the main reasons of disability, reduced life expectancy, and economic cost associated with diabetes [1]. Diabetic neuropathy (DN) is one of the most common and debilitating complications of diabetes, affecting 50–60% of patients with type 1 and type 2 diabetes, although neurophysiological alterations are found in a majority of patients. It may eventually result in foot ulcerations and lower limb amputations, accounting for up to 15% of this type of intervention [2].

There are different forms of DN, but the most common presentation is a chronic sensorimotor polyneuropathy. Patients develop abnormal sensory perception, including paraesthesia, reduced sensitivity to touch and temperature, and pain hypersensitivity and spontaneous burning sensation in a "stocking-and-glove" pattern [2,3]. DN is characterized by a progressive distal-to-proximal degeneration of peripheral nerves, comprising axonal dying-back degeneration, fibre loss, segmental demyelination, remyelination, and abnormal regenerative sprouts. Diabetic nerves develop vascular abnormalities, leading to reduced blood flow and hypoxia [4].

The exact mechanism that leads to the development of DN in type 2 diabetes is not completely known yet, but there is evidence that connects hyperglycaemia and dyslipidaemia with the activation of multiple downstream pathways, like polyol pathway (hyperglycaemia), increased reactive oxygen species (ROS) formation and inflammation, glycation, and metabolic flux dysregulation, collectively resulting in endoplasmic reticulum (ER) and mitochondrial dysfunction, impaired transport, and abnormal neurotrophic signalling in dorsal root ganglia (DRG), and autonomic ganglia neurons, axons and Schwann cells [5]. There is no cure for DN other than strict glycaemic control, dietary changes, and exercise and management of neuropathic pain [3]. However, glucose control alone in type 2 diabetic patients has shown modest or no effect on preventing the progression of DN in large clinical trials [6]. On the other hand, studies involving more than 11,000 individuals from different countries consistently demonstrated that obesity is independently associated with neuropathy [7]. Multiple molecular abnormalities may contribute to DN, and its treatment may require multiple strategies, including neuroprotection and repair.

Over the past decade, with the introduction of high-throughput gene expression profiling assays and, more recently, metabolomics, the molecular landscape of the peripheral nervous system (PNS) of

[1]Institute of Neurosciences, Univ. Autònoma de Barcelona, Spain [2]Department of Biochemistry and Molecular Biology, Univ. Autònoma de Barcelona, Spain [3]Department of Cell Biology, Physiology and Immunology, Univ. Autònoma de Barcelona, Spain [4]Institut Català de Recerca i Estudis Avançats (ICREA), Barcelona, Spain [5]Centro de Investigación Biomédica en Red Enfermedades Neurodegenerativas (CIBERNED), Spain [6]Unitat Mixta UAB-VHIR, Vall d'Hebron Institut de Recerca (VHIR), Barcelona, Spain

*Corresponding author. Institute of Neurosciences, Edifici H, Universitat Autònoma de Barcelona, E-08193, Bellaterra, Spain. E-mail: assumpcio.bosch@uab.cat (A. Bosch).

Received July 8, 2021 • Revision received October 27, 2021 • Accepted November 26, 2021 • Available online 30 November 2021

https://doi.org/10.1016/j.molmet.2021.101408

diabetic murine models [8–12] and diabetic patients [13] has been studied. To our knowledge, there are no studies exploring the effect of type 2 diabetes on the nervous system proteome. Poor correlation between transcriptomics and proteomics results has been demonstrated, supporting the need for a multi-strategy approach [14]. In the current study, we used the BKS-*db/db* mice which bear a mutation in the leptin receptor and show the typical characteristics of type 2 diabetes. It is one of the few type 2 diabetes mouse strains that spontaneously develops DN [15]. We characterized the proteome of lumbar DRG and sciatic nerve (SCN) of these mice at the beginning of DN development by TMT labelling and LC/MS/MS analysis to gain further understanding of the effects of the disease and to elucidate new targets for the development of advanced therapeutic strategies. Proteomic results were validated by western blot, selecting relevant differentially expressed proteins.

2. RESEARCH DESIGN AND METHODS

Experimental design is presented in Supplementary Figure 1.

2.1. Animals

Male BKS-Lepr$^{db/db}$ (Envigo, Horst, The Netherlands) and Lean littermate (BKS-Lepr$^{wt/wt}$) mice were used. We chose males over females since male *db/db* mice develop a more severe form of neuropathy [16]. The *db/db* mouse develops obesity from 4–5 weeks of age, insulin resistance and hyperglycaemia at 4–8 weeks of age. Mice were fed *ad libitum* with a standard diet (2014 Teklad Global; Envigo) and kept under a light–dark cycle of 12 h. Diabetes was assessed by measuring fasting blood glucose weekly with a Glucometer Contour® XT (Bayer, Leverkusen, Germany). Animals with glycaemia below 250 mg/dL were not included in further studies. Biochemical parameters were measured by the Veterinary Clinical Facility (UAB, Bellaterra, Spain). Animal care and experimental procedures were approved by the Biosafety and the Ethical Committees of the Universitat Autònoma de Barcelona.

2.2. Electrophysiology testing

Nerve conduction tests were performed after 12, 17, 21, and 25 weeks of diabetes. Under anaesthesia with pentobarbital (50 mg/kg i.p.), the sciatic nerve was stimulated percutaneously through a pair of needle electrodes placed first at the sciatic notch and then at the ankle, delivering pulses of 0.05 ms up to 25% above the intensity that gave a maximal response. The compound muscle action potential (CMAP) was recorded from the third interosseus plantar muscle with microneedle electrodes. The sensory compound nerve action potential (CNAP) was recorded from caudal nerves by stimulating at a distal site and recording with microneedles placed at the base of the tail. Evoked action potentials were amplified and displayed on a storage oscilloscope (Tektronix 420, Berkshire, UK). The nerve conduction velocity (NCV) was calculated for each segment tested: motor NCV (MNCV) for the sciatic notch-ankle segment and sensory NCV (SNCV) for a 35-mm segment from the tail. During electrophysiological tests, the animals were placed over a warm flat steamer to maintain body temperature [17].

2.3. Sweating test

Mice were immobilized in a plastic tube and sweating was stimulated by subcutaneous injection of pilocarpine nitrate (5 mg/kg), which induces a maximal sweating response. A silicone mould of the plantar surface of the hindpaw (Silasoft Normal, Detax, Ettlingen, Germany) was done after 10 min of stimulation to determine the number of active sweat glands (aSG) and the estimated sweat output (SO) per secreting gland [18].

2.4. Morphometry of tibial nerve

Tibial nerve segments taken above the ankle were fixed in glutaraldehyde-paraformaldehyde (3%:3%) in cacodylate buffer 0.1 M, post-fixed with 1% OsO_4 + 0.8% potassium hexacyanoferrate in PBS, dehydrated with acetone, and embedded in SPURR resin (Sigma-Aldrich, St. Louis, MO, US). Light microscopy images were acquired on 0.7-μm-semithin sections stained with toluidine blue, under a Nikon ECLIPSE 80i microscope. Three to four fields, covering at least 300 myelinated fibres, were randomly selected for morphometrical analyses using ImageJ and ObjectJ plugin [17].

2.5. Cutaneous innervation evaluation

Plantar pads were fixed overnight with 4% PFA-PBS and cryoprotected in 30% PBS-sucrose for 48 h. Fifty μm thick cryotome pad sections were incubated with PGP9.5 antibody, and intraepidermal nerve fibres (IENFs) were counted under fluorescence microscopy [17]. Representative images from footpads were taken under a Nikon Eclipse 90i microscope to quantify the sweat gland area (SGA) and the percentage of immunoreactive area using ImageJ software [19].

2.6. Immunohistochemistry

Anesthetized animals were perfused with 4% PFA-PBS buffer. DRG and SCN were cryoprotected with 30% sucrose and embedded in Tissue-Tek OCT compound (Sakura, Alphen aan den Rijn, Netherlands) to obtain 10-μm-thick sections. Fluorescence signal was detected with a laser confocal microscope ZEISS LSM 700. Antibodies list is in Supplementary Table 1.

2.7. Relative protein quantification using TMT-LC/MS/MS and bioinformatics analysis

Proteomic study was performed independently with DRG and SCN at 15 weeks of diabetes by CSIC/UAB Proteomics Facility. Six pools were prepared using two samples in each pool, thus obtaining three pools for each condition. Eighty μg of protein in RIPA buffer was digested by Filter Aided Sample Preparation (FASP) method [20] using 200 mM triethylamonium bicarbonate buffer. Each digested pool was labelled using different TMTsixplex™ reagents (ThermoFisher, Waltham, MA, US). Amine-reactive Thermo Scientific TMT™ Isobaric Mass Tagging reagents enable multiplex quantitation of proteins using tandem mass spectrometry. Sample fractionation using a SCX ion-exchange column was performed to reduce sample complexity. Samples were injected using a C18 column and an analytic column connected on-line to the high-resolution mass spectrometer LTQ-Orbitrap XL (ThermoFisher). Peptide identification was performed using the Proteome Discoverer v1.4 software (ThermoFisher) under 1% false discovery rate (FDR) criterion and using Uniprot 2017-10 database from *Mus musculus*. Protein quantification was done based on the intensity of reporter ions labelled with TMT and considering only the unique peptides. Venn diagram was generated using Venny [21]. Characterization of protein localization was done using WebGestalt platform [22], whereas functional enrichment analysis was performed by DAVID bioinformatics resources 6.8 [23]. Functional data was validated with String v11.0 [24] and GeneRanker (Genomatix, Munich, Germany) software.

2.8. Real time PCR

Lumbar DRG and SCN were homogenized separately with Tissue Lyser LT at 50 Hz using QIAzol (Qiagen, Hilden, Germany) to obtain total RNA. Messenger RNA was retrotranscribed using iScript™ cDNA Synthesis

Table 1 — Summary of metabolic, electrophysiological, and morphometric parameters, sweat output test and IENFD and SG innervation in male *db/db* mice compared to lean control.

Parameter	Metabolic parameters	
	Lean	*Db/Db*
Weeks of age	21	21
Weeks of diabetes	-	15
Body weight (g)	27.85 ± 0.80	37.83 ± 1.48[d]
Fasting blood glucose (mg/dL)	177.78 ± 9.87	HI (>600 mg/dL)
Fructosamine (mmol/L)	271.14 ± 3.90	372.53 ± 13.53[c]
Free fatty acids (mmol/L)	0.84 ± 0.06	1.09 ± 0.06[a]
Weeks of age	31	33
Weeks of diabetes	-	25
Body weight (g)	30.33 ± 2.12	29.93 ± 3.47 ns
Fasting blood glucose (mg/dL)	188.6 ± 6.39	523.4 ± 17.46[d]
Fructosamine (mmol/L)	258.9 ± 17.75	361.2 ± 29.50[c]
Free Fatty acids (mmol/L)	0.65 ± 0.07	1.05 ± 0.11[b]

#Parameter	Electrophysiological parameters			
	Db/Db			
Weeks of diabetes	12	17	21	25
CMAP	86.57 ± 2.84[a]	70.83 ± 4.55[b]	71.64 ± 5.89[b]	67.89 ± 9.38[b]
MNCV	85.16 ± 6.20[a]	72.25 ± 6.94[b]	78.42 ± 8.76[a]	84.19 ± 4.68[a]
CNAP	96.29 ± 7.97 ns	91.31 ± 20.87 ns	56.23 ± 9.43[c]	39.68 ± 7.82[d]
SNCV	85.00 ± 1.62[c]	92.51 ± 3.93 ns	77.74 ± 2.71[d]	66.01 ± 1.02[d]

#Percentage of change compared to lean mice

Parameter	Morphometric parameters	
	Lean	*Db/Db*
Weeks of diabetes	-	25
G-ratio (perimeter)	0.626 ± 0.004	0.666 ± 0.008[b]
Myelin thickness (μm)	1.729 ± 0.062	1.579 ± 0.046[a]
Myelinated fibres/mm^2	46,947 ± 4105	58,953 ± 1454[a]

Parameter	Sweat output test	
	Lean	*Db/Db*
Weeks of diabetes	-	12
Number of active SG	328.7 ± 8.53	272.0 ± 15.35[a]
SO/active SG	0.49 ± 0.04	0.24 ± 0.08[b]

Parameter	Footpad PGP9.5 staining	
	Lean	*Db/Db*
Weeks of diabetes	-	15
SGA (μm2)	16723.14 ± 1186.37	12094.98 ± 1037.85[b]
% innervated SGA	32.99 ± 1.93	24.97 ± 2.80[a]
IENFD (NNF/mm)	50 ± 2.30	24 ± 7.68[b]

n = 6–9 animals per group for metabolic parameters, n = 3–5 animals per group for morphometric parameters and n = 7–13 animals per group for electrophysiology, sweating test and immunohistochemistry.

[a] $p < 0.05$.

[b] $p < 0.01$.

[c] $p < 0.001$.

[d] $p < 0.0001$, by Student's T test.

Kit, and the analysis of expression was performed by CFX96 Touch™ Real-Time PCR Detection System with SYBR® Green Master Mix (Bio-Rad, Hercules, CA, US). Amplifications were as follows: heat activation (3 min, 95 °C), followed by 39 cycles of 95 °C (10 s) and 58 °C (30 s). Quantification relative to *Rplp0* and *Ywhaz* controls was calculated using the Pfaffl method. Primers' list is in Supplementary Table 2.

2.9. Western blot

DRG and SCN, contralateral to those used in proteomic analysis, were sonicated and homogenized in RIPA lysis buffer with Tergitol NP-40 (Sigma-Aldrich) and Protease Inhibitor Cocktail (Merck, Darmstadt, Germany). Protein concentration was determined by Pierce™ BCA Assay (ThermoFisher). Ten to 20 μg of the sample was separated on 10% SDS-polyacrylamide gel electrophoresis. Immunoreactive proteins were detected by ETA C Ultra 2.0 ECL (Cyanagen, Bologna, Italy) and the ChemiDoc MP Imaging System (Bio-Rad). Protein bands were quantified by densitometry using ImageJ and the results were normalized by actin or tubulin. Antibodies list is in Supplementary Table 3.

2.10. Preparation of BSA-conjugated palmitate

Conjugation protocol from Seahorse Bioscience (Agilent, Santa Clara, CA, US) was followed using Ultra Fatty Acid Free BSA (Roche, Merck) and sodium palmitate (Sigma-Aldrich) to obtain 6:1 M ratio Palmitate:BSA. NSC-34 (motoneuron) and ND7/23 (DRG) hybrid cell lines were selected to study the effect of palmitate *in vitro*. As negative controls,

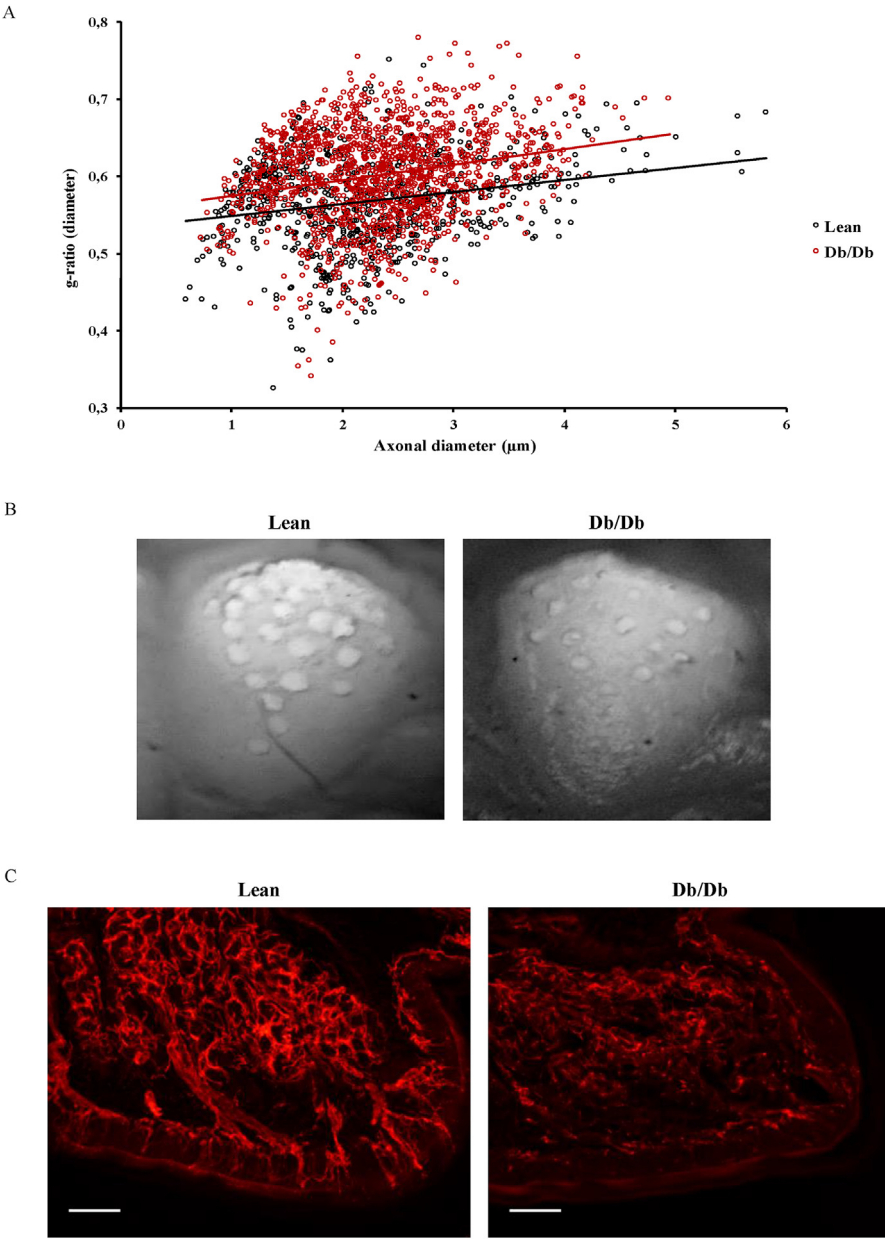

Figure 1: Peripheral neuropathy profiling. A: G-ratio (axonal diameter/fibre diameter) versus axonal diameter (µm) plot from the whole set of analysed nerve fibres showing higher g-ratio due to thinner myelin in *db/db* compared with lean mice. B: Photographs of representative silicone moulds of one footpad with retained impressions of sweat droplets at 10 min after pilocarpine administration, showing that the number of active sweat glands (SG) and the sweat output per gland (SO/active SG) was lower in *db/db* mice. C: Fluorescence images of PGP9.5-immunostained plantar pads showing that intraepidermal nerve fibers and innervation of sweat glands were reduced in *db/db* mice. Scale bar = 100 µm.

BSA and methyl palmitate (non-metabolisable form of palmitate, Sigma-Aldrich) were produced following the same protocol, and thapsigargin (Sigma-Aldrich) was used as a positive inductor of ER stress.

2.11. *Xbp1* alternative splicing

RNA from cell lines was obtained following the same protocol as for tissue samples. Endoplasmic reticulum stress was evaluated by qPCR using primers list in Supplementary Table 2 and by *Xbp1* mRNA alternative splicing. *Xbp1* splicing was assessed by conventional PCR: heat activation (95 ^{o}C, 5 min), followed by 30 cycles of 95 ^{o}C (1 min), 62 ^{o}C (30 s) and 72 ^{o}C (30 s), and a final step of 72 ^{o}C for 10 min. Primers used enabled the amplification of both transcript variants, unspliced *Xbp1* (*uXbp1*, 330 bp) and spliced *Xbp1* (*sXbp1*, 304 bp): Fwd, 5′-TGAGAACCAGGAGTTAAGAACACGC-3′; Rv, 5′-TTCTGGGTA-GACCTCT GGGAGTTCC-3′. PCR products were run into a 7% acrylamide gel.

2.12. Statistical analysis

Data are expressed as mean ± SEM. Electrophysiological, functional and histological results were analysed using Student's t test comparing *db/db* to lean mice, or two-way ANOVA followed by Bonferroni post-

hoc test. For proteomic analysis, differentially expressed proteins were determined using DanteR software [25] performing one-way ANOVA test followed by Benjamini & Hochberg correction to control the FDR. Differences were considered significant when $p < 0.05$.

3. RESULTS

3.1. Peripheral neuropathy profile

Ninety four percent of *db/db* males spontaneously developed diabetes at 9 weeks of age as a result of severe obesity. *Db/db* mice showed progressive increase in weight and glycaemia, reaching values over 50 g and 600 mg/dL, respectively, until 12 weeks of diabetes, then started to lose weight, despite sustained hyperglycaemia and high levels of serum free fatty acids and fructosamine (Table 1). This phenomenon was observed in multiple batches of animals.

We characterized DN in these animals by electrophysiological and sweating tests, nerve histology and cutaneous innervation (Figure 1, Table 1). We observed a consistent decline in CMAP amplitude and MNCV from the first time point analysed (12 weeks of diabetes) in the *db/db* mice, whereas values were maintained in the lean mice. Sensory caudal nerve conduction also showed a progressive decline with a marked reduction at 25 weeks. Morphometric characterization of tibial nerves showed a higher g-ratio due to thinner myelin in *db/db* at 25 weeks compared with lean mice, corresponding to the decline of NCV. Morphometric analysis at previous time points did not detect any difference (data not shown). We also observed higher myelinated fibre density in tibial nerves from diabetic mice as well as a shift towards smaller diameter fibres in *db/db* mice (Figure 1A). These changes may indicate a degeneration of large fibres followed by a regenerative process that increases the number of smaller myelinated fibres [26,27]. Disorders of sweating, caused by degeneration of post-ganglionic sudomotor axons, are common in DN [28]. In agreement, the number of aSG and the SO per gland was lower in *db/db* than in lean mice already at 13 weeks of diabetes (Figure 1B, Table 1), indicating full denervation of some SG and partial denervation of still responsive glands. Loss of innervation of SG was confirmed by immunolabelling against PGP9.5 of plantar pads (Figure 1C). Diabetic mice showed a significant reduction of SGA innervation and of the IENFD, confirming a distal autonomic and sensory neuropathy [29].

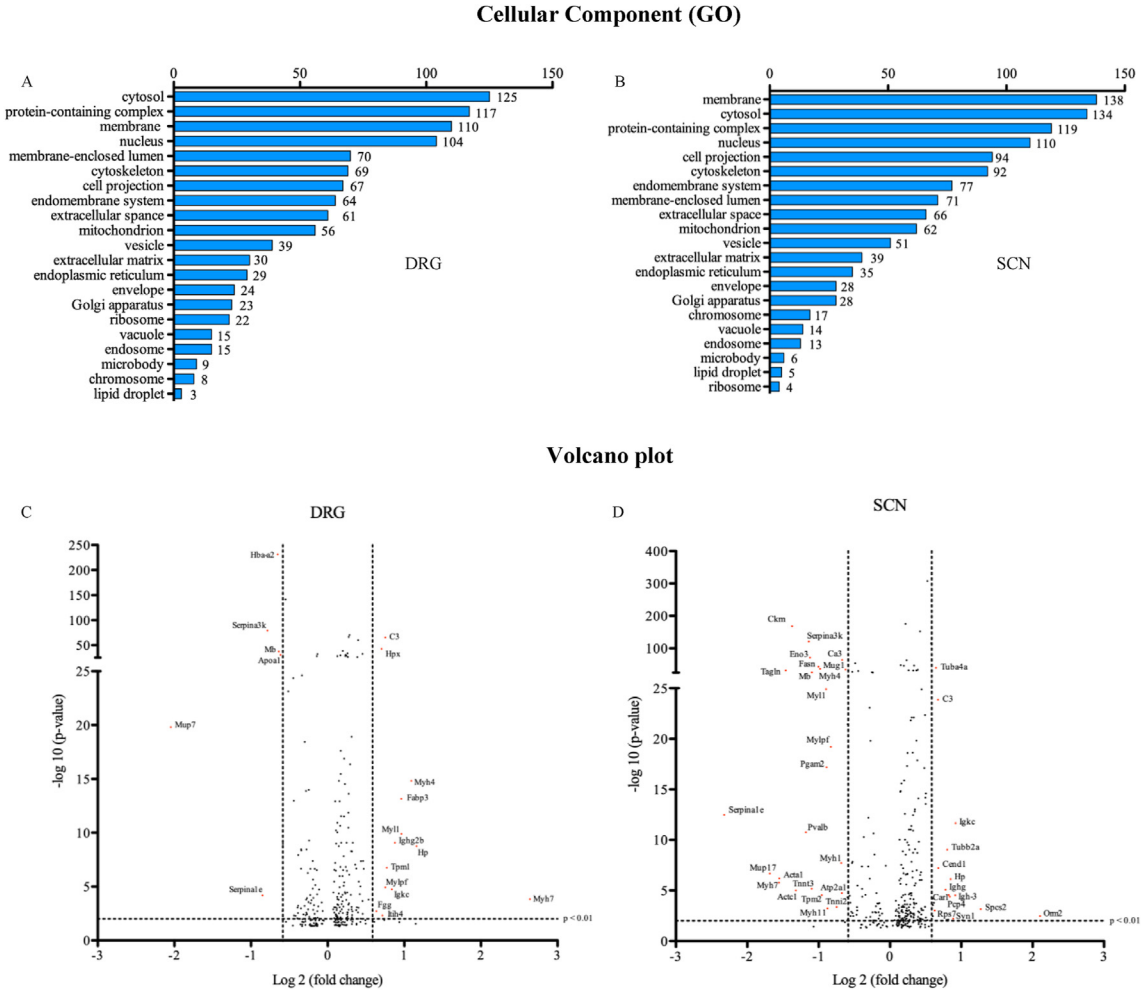

Figure 2: Proteomic dataset characterization. A, B: Cellular component categories plot of DRG and SCN data obtained using WebGestalt software and gene ontology database. C, D: Volcano plot showing statistical significance ($-\log_{10}$ *p*-value) versus magnitude of change ($\log_2$ fold change) of the whole dataset from DRG and SCN. In a volcano plot, the most upregulated genes are towards the right, the most downregulated genes are towards the left, and the most statistically significant genes are towards the top. Differentially expressed proteins with a fold change $\geq$1.5 or ≤ -1.5 and a *p*-value < 0.01 are highlighted in red.

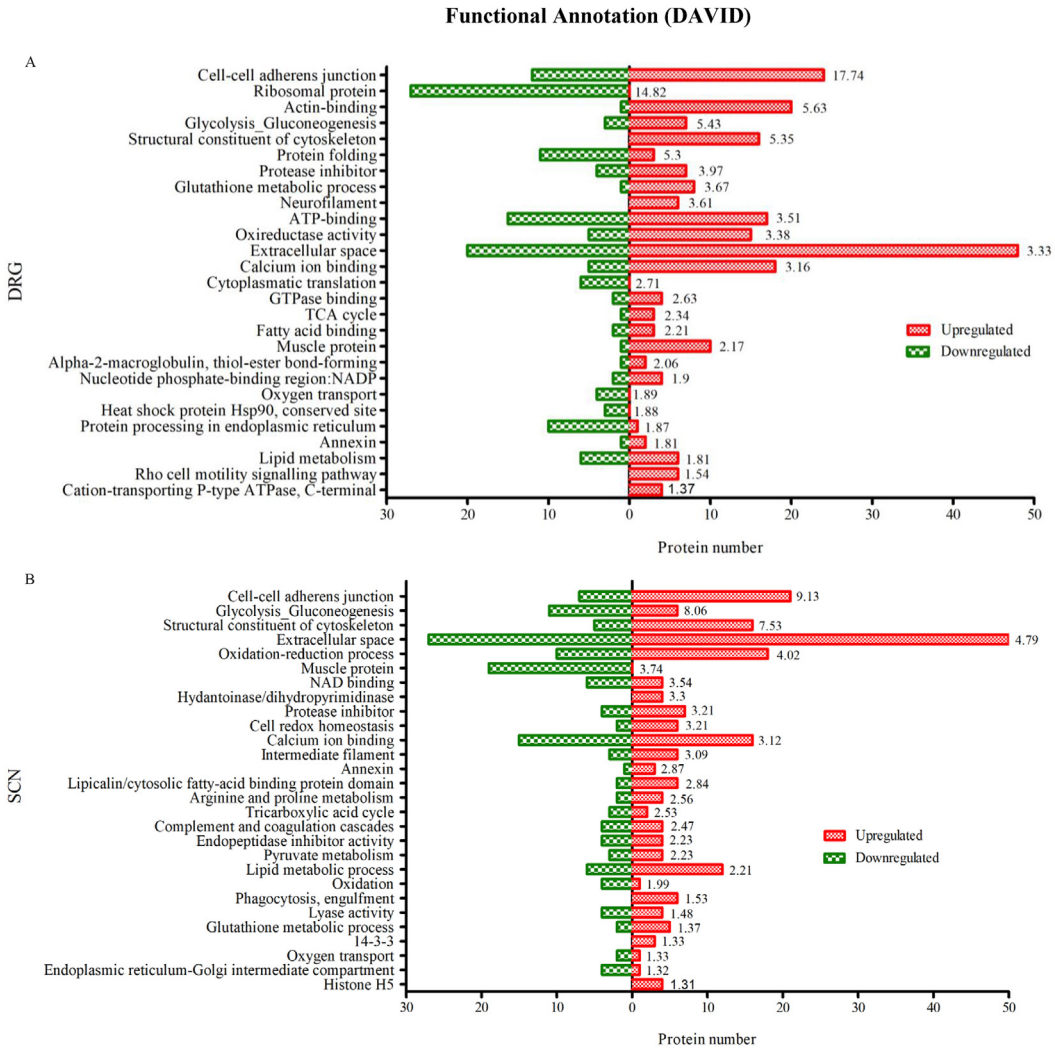

Figure 3: Functional annotation analysis. A, B: Most relevant functional clusters obtained by DAVID 6.8 analysis are represented for DRG and sciatic nerve data. In red, proteins upregulated and, in green, downregulated proteins for each biological term are shown. Functional clusters are ordered according to an enrichment score for the group, based on the geometric mean of annotation terms' *p*-values.

3.2. Functional enrichment

Based on electrophysiological and morphometric data, we selected *db/db* mice with 15 weeks of diabetes to characterize the DRG and SCN proteome before morphometric changes were detected. A proteomic study of DRG identified 866 proteins, whereas in SCN we found 843. DanteR software determined 286 and 312 differentially expressed proteins for DRG and SCN, respectively between *db/db* and lean males (one-way ANOVA following by Benjamini & Hochberg correction for multiple testing). Regarding DRG, 185/286 proteins were upregulated and 101 downregulated. Of those, 68 proteins showed ratios higher than 1.2, whereas 31 proteins were downregulated below ratios of 0.8. Concerning SCN, 217/312 proteins were increased, 117 of which with a ratio higher than 1.2. 95 were downregulated, 57 with a fold change lower than 0.8.

The differentially expressed proteins from DRG and SCN were compared using a Venn diagram, showing a 34.3% of proteins shared between both data sets (Supplementary Figure 2).

We used WebGestalt to characterize protein localization based on subcellular categories from Gene Ontology and volcano plot to identify those genes with larger fold changes that were also statistically significant (Figure 2). We used DAVID 6.8 to identify the most significant biological functions in the datasets. Functional annotation clustering allowed to pool similar biological processes, focussing on enrichment scores higher than 1.3 ($p < 0.05$). Figure 3 shows the most relevant functional clusters obtained by DAVID analysis and the number of proteins found up or downregulated for each biological term.

To generate a pathway network of interconnected proteins, we used String software (Supplementary Figure 3 and Supplementary Tables 4 and 5). In DRG, the network consisted in 221 nodes and 539 edges with an enrichment *p*-value <1.0e-16, indicating that these proteins are at least partially biologically interconnected. The protein association network from SCN involved 308 nodes connected through 654 edges, also with significantly more interactions than expected.

We analysed datasets using GeneRanker software to perform a similar analysis as DAVID but in an automated way, using conventional databases and existing bibliography as data source. We selected biological functions derived from GO-terms as the most relevant information (Supplementary Tables 6 and 7).

Table 2 — DRG proteins highlighted in the results section are shown with the corresponding fold change ratio and grouped by functional clusters.

DRG		
Oxidative stress	**60S ribosomal proteins**	**Acute-phase response (positive)**
GSTM1 (1.32)	P2 (0.89)	Haptoglobin (2.23)
GSTM2 (1.10)	L4 (0.83)	Orosomucoid 1 (1.52)
GTSM5 (1.37)	L7 (0.88)	Fibrinogen gamma chain (1.55)
IDH2 (1.35)	L7a (0.87)	Complement C3 (1.68)
SOD1 (1.13)	L10a (0.79)	Hemopexin (1.63)
Glyoxalase I (1.12)	L13 (0.88)	Inter-alpha-inhibitor heavy chain 4 (1.64)
Peroxiredoxin-1 (1.08)	L17 (0.82)	
Peroxiredoxin-6 (1.11)	L21 (0.75)	**Acute-phase response (negative)**
	L30 (0.86)	Serum albumin (0.91)
Glycolitic pathway	L31 (0.79)	Alpha-2-HS-glycoprotein (0.91)
Beta enolase (0.79)	L32 (0.82)	
Phosphoglycerate mutase 2 (0.76)	L34 (0.78)	**Inflammatory markers**
	L35a (0.82)	S100-A8 (1.32)
Lipid catabolism	L38 (0.87)	S100-A9 (1.34)
Trifunctional enzyme (1.19)		Ig light chain kappa (C region) (1.79)
Acetyl-CoA acetyltransferase (1.10)	**40S ribosomal proteins**	Ig heavy chain gamma 2B (C region) (1.84)
	S2 (0.9)	
Lipid biosynthesis	S3 (0.87)	**Protein folding**
17-beta-HSD 12 (0.76)	S4 (0.82)	PPlase A (1.15)
Fatty acid synthase (0.74)	S5 (0.7)	Alpha(B)-crystallin (1.32)
NADP-dependent malic enzyme (0.87)	S7 (0.79)	HSP84 (0.82)
	S13 (0.79)	Protein disulfide-isomerase A3 (0.91)
Muscle-type and cytoskeleton	S16 (0.86)	Heat shock cognate 71 kDa protein (0.91)
Myosin heavy chain-4 (2.13)	S19 (0.88)	HSP86 (0.81)
Myosin light chain-1 (1.95)		Endoplasmin (0.89)
Tropomyosin-2 (1.91)	**Translation factors**	Chaperonin 10 (0.86)
Myosin regulatory light chain 2 (1.68)	eIF-4A-II (0.85)	Chaperonin 60 (0.89)
Actin (1.39)	EF-1-gamma (0.84)	Hsc70-interacting protein (0.91)
Neurofilament light polypeptide (1.22)	EF-1-alpha-2 (0.93)	TCP-1-delta (0.77)
Neurofilament heavy polypeptide (1.20)		Calreticulin (0.88)
Tubulin beta-5 chain (1.25)	**Highlighted proteins**	Calnexin (0.86)
Tubulin beta-2A chain (1.24)	SERCA1 (1.67)	GRP-78 (0.95)
Tubulin alpha-4A chain (1.21)	ANT1 (0.73)	
Tubulin beta-4B chain (1.18)	Creatine kinase M-type (0.88)	
Tubulin beta-4A chain (1.18)	V-type ATPase subunit H (0.67)	
Tubulin beta-3 chain (1.16)	MUP7 (0.24)	
Tubulin alpha-1A chain (1.12)		
Spectrin beta chain (1.08)		
Spectrin alpha chain (1.07)		
Moesin (1.09)		

Different software obtained similar biological conclusions from our proteomic datasets, concluding that *db/db* DRG and SCN develop metabolic dysregulation related to glucose and lipid metabolism, tissue scaffold abnormalities based on alterations in structural proteins, a mild dysregulation of folding chaperones, an upregulation of acute-phase response and inflammation, and an alteration of oxidative stress-related proteins.

3.3. Validation of the proteomic results

DRG and SCN proteins highlighted in this section are shown in Tables 2 and 3 grouped by functional clusters with the corresponding fold change. We found multiple proteins involved in glutathione metabolism and antioxidant activity in both tissues. In DRG, several isoforms belonging to Mu class of Glutathione S enzymes (GSTM) were upregulated, whereas in SCN, some of these isoforms were reduced. These opposite results were confirmed by western blot in both tissues (Figure 4A—D). Conjugated with glutathione, GSTM participates in the detoxification of electrophilic compounds, including products of oxidative stress. Concomitantly, we observed that mitochondrial isocitrate dehydrogenase 2, which promotes regeneration of reduced glutathione by supplying NADPH [30], was increased in DRG (Table 2) but not in SCN. On the other hand, in both tissues we found an increase of superoxide dismutase 1 and many peroxiredoxins isoforms, a highly-conserved family of antioxidant proteins that scavenge cellular ROS. Other antioxidant proteins, such as thioredoxin, glutaredoxin-1, and glyoxalase I, were found augmented.

Lipid and carbohydrate metabolism were also altered in both tissues. Several enzymes implicated in glycolytic pathway (phosphoglucose isomerase, phosphofructokinase, ß-enolase, phosphoglycerate mutase 2, phosphoglycerate kinase 1, GAPDH and fructose biphosphate aldose 1) were downregulated. In SCN, we observed a decline in the content of aconitase, a TCA cycle enzyme. In SCN we also detected decreased levels of OGDC-E2, which catalyses the conversion of 2-oxoglutarate to succinyl-CoA and CO_2 in the TCA cycle (Table 3). Regarding lipid metabolism, we found an upregulation in lipid catabolism-related proteins (trifunctional enzyme, acetyl-CoA acetyltransferase, perilipin-1, monoglyceride lipase, Ras-related protein Rab-7a and Enoyl-CoA delta isomerase I), whereas a reduction in proteins implicated in lipid biosynthesis (17-ß-HSD 12, fatty acid synthase, NADH-cytochrome b5 reductase 3 and NADP-dependent malic enzyme).

Translation was downregulated in DRG as demonstrated by a decrease in proteins that constitute the ribosomal subunits 60S and 40S and the translation-related factors eIF-4A-II, EF-1-gamma and EF-1-alpha-2

Table 3 — SCN proteins highlighted in the results section are shown with the corresponding fold change ratio and grouped by functional clusters.

SCN		
Oxidative stress	**Muscle-type and cytoskeleton**	**Acute-phase response (positive)**
GSTM2 (0.69)	Myosin heavy chain-4 (0.51)	Haptoglobin (1.81)
IDH2 (0.9)	Myosin light chain-1 (0.54)	Orosomucoid 1 (1.51)
SOD1 (1.17)	Tropomyosin-1 (0.66)	Complement C3 (1.59)
Thioredoxin (1.22)	Tropomyosin-2 (0.52)	Hemopexin (1.41)
Glutaredoxin-1 (1.19)	Myosin regulatory light chain 2 (0.56)	Inter-alpha-inhibitor heavy chain 4 (1.44)
Glyoxalase I (1.26)	Actin (0.34)	
Peroxiredoxin-1 (1.06)	Neurofilament light polypeptide (1.11)	**Acute-phase response (negative)**
Peroxiredoxin-6 (1.2)	Neurofilament heavy polypeptide (1.11)	Serum albumin (0.75)
Peroxiredoxin-5 (1.23)	Tubulin beta-5 chain (1.25)	Alpha-2-HS-glycoprotein (0.89)
Peroxiredoxin-2 (1.09)	Tubulin beta-2A chain (1.74)	
	Tubulin alpha-4A chain (1.56)	**Inflammatory markers**
Glycolitic pathway	Tubulin beta-4B chain (1.36)	S100-A9 (1.35)
Phosphoglucose isomerase (0.81)	Tubulin beta-4A chain (1.18)	Ig light chain kappa (C region) (1.89)
Phosphofructokinase (0.87)	Tubulin beta-3 chain (1.23)	Ig heavy chain gamma 2B (C region) (1.89)
Beta enolase (0.46)	Tubulin alpha-1A chain (1.29)	Ig heavy chain gamma 2A (C region) (1.71)
Phosphoglycerate mutase 2 (0.54)	Spectrin beta chain (1.10)	Ig heavy chain gamma 1 (C region) (1.46)
Phosphoglycerate kinase 1 (0.86)	Spectrin alpha chain (1.17)	
GAPDH (0.85)	Moesin (1.21)	**Protein folding**
Fructose biphosphate aldose 1 (0.71)		PPlase A (1.15)
	Highlighted proteins	Alpha(B)-crystallin (1.18)
TCA cycle	SERCA1 (0.63)	Prostaglandin E synthase 3 (1.19)
Aconitase (0.89)	ANT1 (0.73)	HspB1 (1.09)
Dihydrolipoamide succinyltransferase (0.72)	Creatine kinase M-type (0.39)	Heat shock cognate 71 kDa protein (1.06)
	MUP17 (0.31)	TCP-1-alpha (1.27)
Lipid catabolism		Protein disulfide-isomerase A3 (0.91)
Acetyl-CoA acetyltransferase (1.18)		PDI (0.93)
Perilipin-1 (0.76)		HSP84 (0.88)
Monoglyceride lipase (1.52)		GRP-78 (0.88)
Ras-related protein Rab-7a (1.10)		
Enoyl-CoA delta isomerase I (1.76)		
Lipid biosynthesis		
Fatty acid synthase (0.50)		
NADH-cytochrome b5 reductase 3 (0.83)		
NADP-dependent malic enzyme (0.68)		

(Table 2), but not in SCN. Another discrepancy between SCN and DRG was the upregulation of muscle-related proteins in DRG, such as myosin heavy chain-4, myosin light chain-1, tropomyosin-1, tropomyosin-2, myosin regulatory light chain 2, and actin (Table 2), but their downregulation in SCN (Table 3). However, cytoskeleton proteins were augmented in both tissues (neurofilament polypeptide, tubulin, spectrin and moesin).

Our data shows differentially expressed positive (haptoglobin, orosomucoid 1, fibrinogen gamma chain, complement C3, hemopexin and inter-α-inhibitor heavy chain 4) and negative, acute-phase proteins (serum albumin and alpha-2-HS-glycoprotein) (Tables 2 and 3). C3 overexpression was confirmed by western blot in both tissues (Figure 4A—D). Many of these proteins can modulate one or more stages of the inflammatory response. Associated with the acute-phase response activation, inflammatory markers like S100-A8/9 in DRG and S100-A9 in SCN were enriched, while levels of immunoglobulin light chain kappa and heavy chain gamma were higher in both tissues.

In addition to the detailed functional clusters, some interesting proteins were highlighted, such as SERCA1, ANT1, V-ATPase subunit H and MUP. SERCA1 (Sarcoplasmic/endoplasmic reticulum calcium ATPase 1) was increased in DRG, but downregulated in SCN (Tables 2 and 3). In agreement with this observation, several molecular chaperones were moderately dysregulated in DRG and SCN such as PPlase A, alpha(B)-crystallin, HSP84, protein disulfide-isomerase A3, heat shock cognate 71 kDa protein, and GRP-78.

Related to energy depletion, ANT1 (ADP/ATP translocase 1), which forms a channel in the inner mitochondrial membrane that allows the translocation of ATP to the cytoplasm, was downregulated in both tissues (Tables 2 and 3). We also observed lower levels of creatine kinase M-type. This enzyme catalyses the reversible interconversion of creatine into phosphocreatine, which is used to keep constant global and local ATP/ADP ratio [31]. ATP exhaustion is probably the cause of the downregulation of V-type proton ATPase subunit H in DRG proteome (Table 2), which was validated by western blot in both DRG and SCN tissues (Figure 4A—D). This multisubunit enzyme is responsible for the establishment of the acidic pH of endocytic and secretory organelles, pumping cytosolic H^+ into their lumen.

MUP (major urinary protein) was the most depleted protein in DRG and the second most downregulated in SCN. MUP is a lipocalin family member secreted to circulation by the liver and filtered by the kidneys into the urine. However, we detected *Mup* mRNA both in DRG and SCN by real time PCR and its expression was much lower in *db/db* compared to lean mice, in agreement with our proteomic results. The decrease in expression was dependent on the time of diabetes in DRG. In SCN, *Mup* expression is almost absent already at 1 week of diabetes, pointing at a very early effect of metabolic syndrome (Figure 5A). This result was corroborated by western blot in both tissues (Figure 4A—D). MUP does not colocalize with neuronal somas nor satellite cells in DRG (Figure 5B), and neither axons nor Schwann cells in SCN (Figure 5C). Alternatively, we detected MUP in the extracellular space, colocalizing with connective tissue in DRG and with endoneurium in SCN, as observed by collagen IV colocalization (Figure 5D), which adds relevance to the important changes found in proteins related to extracellular space (Figure 3).

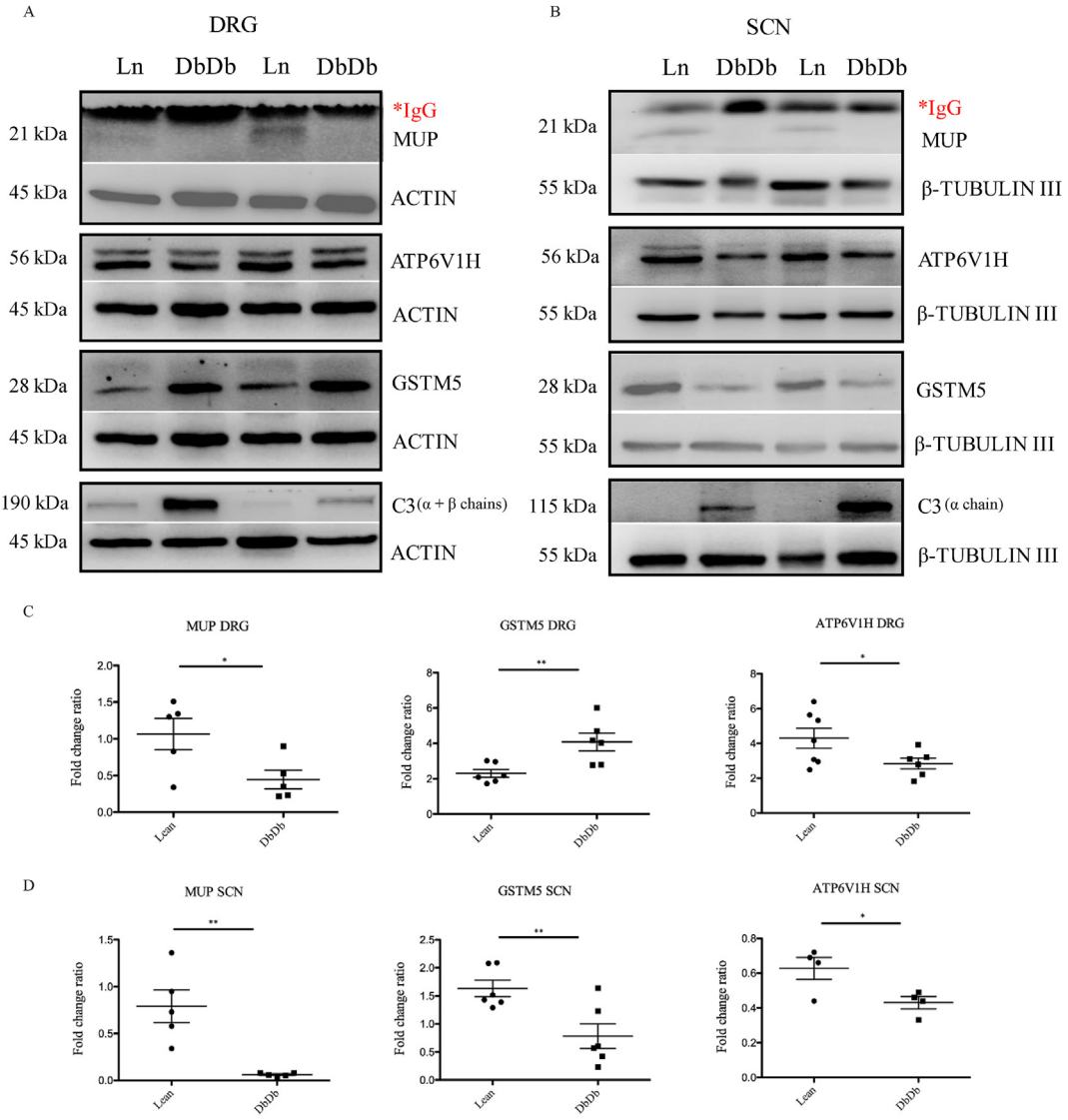

Figure 4: Western blot validation of proteomic data. A, B: MUP, ATP6V1H, GSTM5 and C3 proteins were selected to validate proteomic results using blot immunodetection based on their relevance in oxidative stress, inflammation or due to its new potential role in the peripheral nerve. Representative western blots of these proteins are shown for DRG and SCN at 15 weeks of diabetes. C, D: We found statistically significant differences between *db/db* and lean mice using a sample size of 4–7 mice (*$p < 0.05$, **$p < 0.01$ by Student's t test) and, moreover, these correlate with the results obtained by mass spectrometry.

4. DISCUSSION

Proteomic studies are of interest in deciphering the pathophysiological mechanisms and guiding the search for preventive strategies of diseases. We identified several altered pathways in the PNS of *db/db* mice, with most relevance in those related to oxidative stress, metabolic dysregulation, ribosomal proteins, muscle-type and cytoskeleton proteins, and acute phase and inflammatory and UPR responses.

No other proteomic studies have been reported so far for DN in type 2 diabetes. Using microarray technology, Pande et al. [8] characterized the transcriptional profile of the SCN from *db/db* mice at 20 weeks of diabetes. They identified several pathways enriched in diabetic animals: carbohydrate and lipid metabolism, glutathione metabolism, cell development, cell adhesion and extracellular matrix-receptor interaction, and signal transduction pathways. We found similar biological annotations but also some discrepancies between transcriptomic and proteomic data regarding fold change directionality that may be due in part to differences between both studies, as we used animals with shorter duration of diabetes, and lean instead of heterozygous (db/+) mice as controls.

4.1. Oxidative and ER stress

Several proteins involved in glutathione metabolism and antioxidant activity are altered in our study, supporting the hypothesis that oxidative stress has an important role in DN aetiology [5]. In the same model, Hinder et al. [9] described increased levels of 3-nitrotyrosine and HODEs in DRG and SCN, markers of protein oxidation and lipid peroxidation, respectively. It is also remarkable the increase of glyoxalase I, as it participates in the elimination of methylglyoxal, a toxic compound derived from glucose metabolism in hyperglycaemic conditions [32]. In diabetes, oxidative stress and saturated fatty acids reduced SERCA activity [33,34]. In agreement

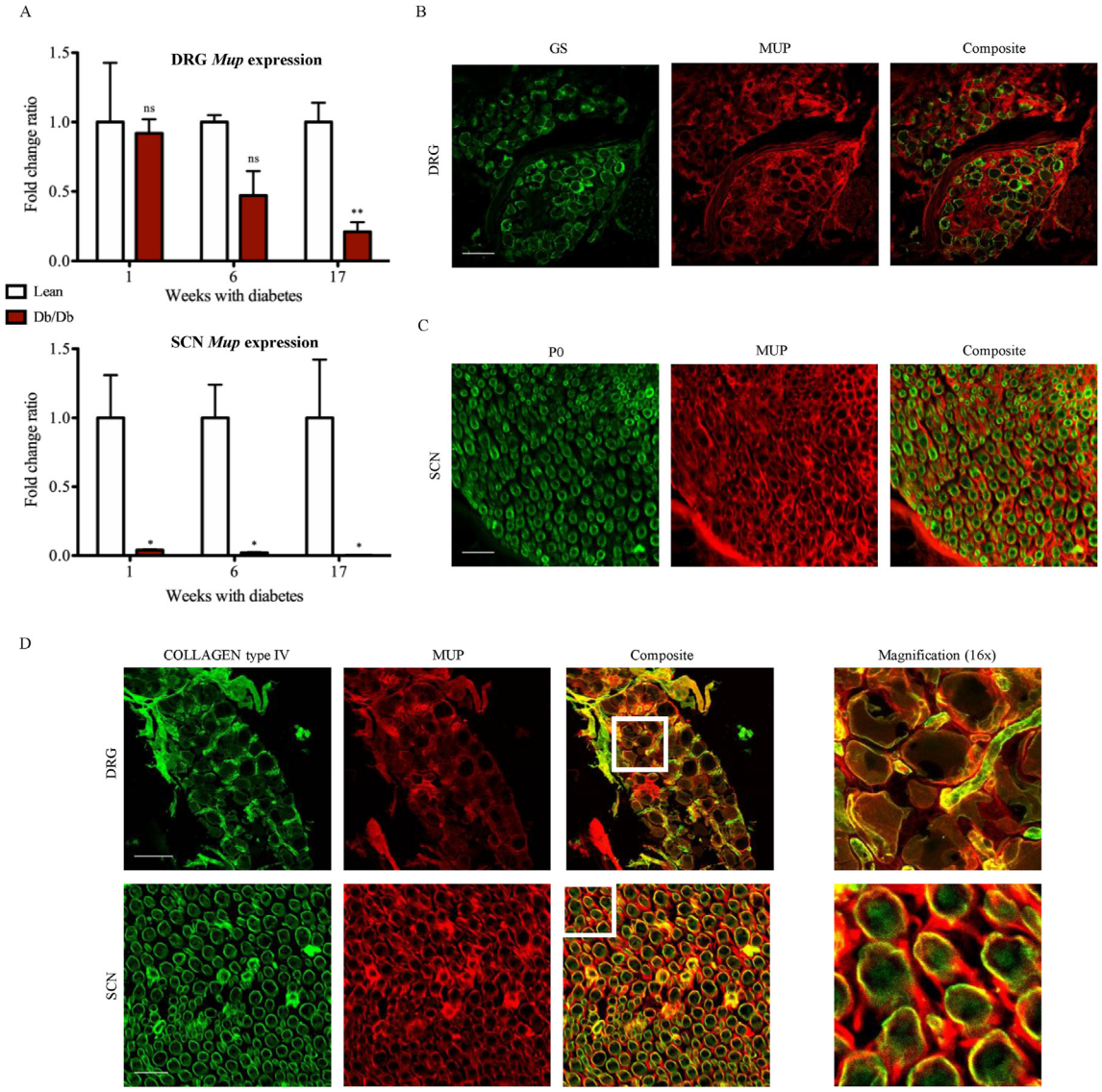

Figure 5: MUP localization in PNS. A: *Mup* gene expression was evaluated by qPCR in DRG and SCN at three different time points (one, six and seventeen weeks after diabetes onset) observing a progressive decline in its expression inversely correlating with the time of diabetes. Data was normalized to lean mice ($n = 3–4$ animals per group, $^{*}p < 0.05$, $^{**}p < 0.01$, by two-way ANOVA followed by Bonferroni's Post hoc test). B: Satellite cells from lumbar DRG were labelled against glutamine synthetase (green) concluding that MUP (red) does not colocalize with this cell type. Scale bar = 100 μm. C: Schwann cells from SCN were immunodetected using an antibody against P0 (green) indicating that MUP protein (red) was not part of the myelin. Scale bar = 25 μm. D: Extracellular matrix was immunolabelled with collagen type IV (green) in DRG and SCN tissues. Colocalization of collagen type IV and MUP (red) are observed in the magnification (16×) of the composite pictures demonstrating that MUP protein is located in the extracellular matrix of the PNS. Scale bars = 100 μm (DRG) and 25 μm (SCN).

with these data, we found downregulated levels of SERCA1 in SCN, whereas increased in DRG. SERCA1 is a membrane-bound enzyme that transports Ca^{2+} from the cytosol into the ER. Since protein folding is Ca^{2+}-dependent, calcium depletion in the ER leads to protein misfolding, resulting in the activation of UPR to recover homoeostasis [34]. A mild dysregulation in several molecular chaperones was detected in both tissues, which might result in ER homoeostasis disruption [35].

We did not expect the lack of activation of the unfolded protein response in diabetic PNS. Some folding chaperones exhibited lower levels compared to lean animals. These findings are opposite to those observed in proof of concept studies we performed *in vitro* as well as previous bibliography with cultured Schwann cells [36]. Using the cell lines ND7/23 and NSC-34 as in vitro models of sensory and motoneurons, respectively, we tested the activation of unfolded protein response upon palmitate exposure for 12 h. What we observed was a dose—response effect of palmitate on UPR markers such as *Hspa5* (BiP) and *Ddit3* (CHOP) mRNA upregulation and *Xbp1* splicing activation (Supplementary Figures. 4 and 5).

A possible explanation for these results could be related to the difference between acute and chronic exposure to a particular insult. Acute exposure to palmitate may trigger a marked response to counteract the ER stress, whereas chronic exposure may eventually overwhelm the cell capacity leading to blunted UPR.

4.2. Metabolic deficiency

Several enzymes implicated in glycolytic pathways and the TCA cycle were downregulated, coinciding with a previous study reporting the reduction of glycolytic metabolites and lower levels of citrate and isocitrate in *db/db* mice, which may indicate energetic deficiency [9]. In parallel, we found an upregulation in lipid catabolism whereas a decline in lipid biosynthesis, as an effort to increase cellular ATP. The enrichment of genes related to lipid metabolism has also been described by Pande et al. [8], which hypothesized that it could be associated to increased amounts of adipose tissue in the epineurium of the *db/db* mice. Furthermore, Sas et al. [37] described an increase in metabolic flux towards lipid oxidation in SCN from *db/db* mice after 20 weeks with diabetes.

In this regard, lower ATP availability in the PNS of *db/db* mice is also represented by downregulation of ANT1 and creatine kinase M-type (M-CK), in both tissues. Furthermore, ANT1, which is responsible for 50–66% of the basal proton conductance (BPC), has been proposed to protect from oxidative damage by partial dissipation of Δp by mild uncoupling and limiting the formation of ROS [38]. Since ANT1 content is lower, poor BPC may increase superoxide production. The downregulation of V-ATPase subunit H in DRG may also be related to the decrease in ATP concentration. V-ATPase has a role in protein processing and degradation by lysosomes, endocytosis, and vesicular traffic, as well as synaptic vesicle loading, driven by the electrochemical gradient [39].

Transcriptomic and metabolomic studies in type 1 diabetes drew similar conclusions regarding metabolic deficiency in diabetic PNS as type 2 diabetes. Akude et al. [40] demonstrated lower levels of proteins related to TCA cycle and mitochondrial respiratory chain in DRG sensory neurons from STZ-induced diabetic rats after 22 weeks. Rojas et al. [41] detected an evident reduction of some TCA metabolites in sciatic nerve of type 1 diabetic C57 Bl6/j mouse after 22 weeks with diabetes. Overall, it seems that the long-term outcome in type 1 diabetes models may be a metabolic deficiency as described in type 2 diabetes models by previous bibliography and our own data.

4.3. Translational machinery

In DRG, we found a notable decrease in proteins related to translational machinery, especially those that constitute the ribosomal subunits 60S and 40S. This could also be related to ATP depletion or even to insulin resistance, which may decrease the insulin mediated protein synthesis [42]. Ribosomal proteins were not altered in SCN.

4.4. Cytoskeleton and muscle-like proteins

The upregulation of muscle-related proteins in DRG was corroborated by other studies reporting the presence of myosin and troponin in DRG neurons [43,44], while actin and tropomyosin isoforms, the major components of neuronal microfilaments, were increased in DRG following spinal nerve ligation, suggesting that muscle-type enzymes could be upregulated to uphold functional and structural stability of cells under stress [45]. Overall, it seems that there is an alteration of cell scaffold considering also the upregulation of cytoskeleton proteins in both tissues that could be related with injury or inflammation.

4.5. Inflammatory response

Acute-phase response proteins increase or decrease in plasma during inflammatory disorders, modulating the inflammatory response. We found both, positive and negative acute-phase proteins differentially expressed in *db/db* PNS. As in our study, haptoglobin, orosomucoid 1, and C-reactive protein were increased in diabetic patients, whereas serum albumin was also decreased [46]. Orosomucoid 1 (AGP1) is a member of the immunocalin family that modulates immune and inflammatory responses [47], and it is increased in adipose tissue of *db/db* mice and in plasma of obese and/or diabetic patients. Higher AGP1 levels were beneficial in *db/db* mice as it improved insulin tolerance with the suppression of proinflammatory and prooxidative profiles in their adipose tissue [48]. *Agp1* mRNA upregulation in *db/db* DRG has also been described [11]. On the other hand, we found overexpression of complement C3, one of the most versatile complements in host defense and inflammation. Activated complement is present in the microvessels of sural nerve from diabetic patients [49] as well as in murine DRG after spinal nerve ligation [45], suggesting a potential role in myelin clearance after injury [50]. Hemopexin, which may be involved in oxidative stress protection, was also increased in DRG and SCN of *db/db* mice in this study. In injured peripheral nerves, hemopexin mRNA is expressed by fibroblasts, Schwann cells, and invading macrophages, accumulating in the extracellular matrix of SCN and DRG [51]. All these data suggest that the higher levels of acute-phase proteins could be a mechanism of protection against excessive inflammation and oxidative damage in DN. We observed the enrichment of inflammatory markers such as S100-A8/9 with a role in activation of NADPH oxidase and advanced glycation end products (AGEs) receptors, which are involved in the pathogenesis of complications of diabetes [5,52,53]. S100-A8/9 are also associated with a higher risk of developing DN in type 1 diabetic patients [54]. In addition, higher levels of immunoglobulin light chain kappa and heavy chain gamma were also detected. Higher expression of Ig γ chain at RNA level was found in DRG from *db/db* mice, suggesting that upregulation at protein level must be at least partially of neuronal origin [11].

4.6. Major urinary protein

Of note, the most downregulated protein in DRG and the second most downregulated in SCN was MUP, a lipocalin family member that binds to pheromones and other lipophilic molecules and regulates its transport and release into the air from urine marks [55]. *Mup1* mRNA was reduced by 30-fold in the liver of *db/db* mice and decreased in circulation of both high-fat diet (HFD) and *db/db* mice [56]. Recombinant MUP1 suppresses the gluconeogenic and lipogenic programs in the liver [57] and promotes mitochondrial biogenesis and oxidative phosphorylation in skeletal muscles, thus increasing energy expenditure and insulin sensitivity [56]. Furthermore, rosiglitazone and resveratrol, which decrease hyperglycaemia and glucose intolerance in diabetic mice, also stimulate *Mup1* expression in the liver [56,58]. *Mup1* is also expressed in mouse skeletal muscle, and it markedly decreases with HFD but increases with exercise training. Moreover, it improves insulin-stimulated GLUT4 translocation in cultured muscle cells [59]. Here, we demonstrate that MUP is expressed by both SCN and DRG and located in the extracellular matrix of PNS. Its expression inversely correlates with the time of diabetes in DRG and it is a very early event in SCN, which needs further studies. Despite structural similarities with the acute-phase protein AGP1, as observed by the pairwise alignment of both three-dimensional structures, and both belonging to the lipocalin family, we were not able to demonstrate *in vitro* a role of MUP in oxidative stress protection (data not shown). It would be interesting to study the overexpression or downregulation of MUP in the PNS of T2DM and wild-type animals.

4.7. DRG and SCN comparison

Despite the Venn diagram showing a low percentage of common differentially expressed proteins between these two sets, further functional analysis with bioinformatic resources clearly demonstrated

small differences between DRG and SCN proteome under diabetes. Most functional clusters are shared between tissues. To highlight some differences, the antioxidant enzymes like GSTM, the sarco/ER Ca^{2+} ATPase, and the muscle-related proteins are all increased in DRG but not in SCN, which may indicate a higher response to stress by the DRG compared to the SCN. Translational machinery was found decreased in DRG, whereas no changes were detected for SCN. These results correlate with a previous publication that compared transcriptional network from DRG and SCN in type 2 diabetes using microarray analysis without any relevant difference highlighted between them [60].

4.8. Conclusions

In conclusion, our proteomic data uncover new pathways altered in DN and validate previous transcriptomic and metabolomic results, confirming that both DRG and SCN present molecular alterations even before morphometric changes developed. It is worth mentioning that many efforts have been made to develop therapeutic approaches that counteract oxidative stress and inflammation with low or moderate effect in clinical practice. Our results, in conjunction with other publications, point out that low ATP bioavailability due to metabolic impairment could represent the main mechanism of neurodegeneration observed in diabetic neuropathy. These findings may provide important information to select appropriate targets to develop new therapeutic strategies for DN.

It would be interesting to compare the proteomic data from DbDb with obese and prediabetic HFD models, since obesity itself represents an independent risk factor for diabetic neuropathy. This comparison may enable to elucidate the role of obesity before hyperglycaemia develops.

ACKNOWLEDGEMENTS

M.L.J researched data and wrote the manuscript. J.J.V researched data. A.O contributed to animal experiments. S.V contributed to animal experiments and discussion. A.S reviewed/edited manuscript. M.C contributed to discussion and reviewed/edited manuscript. X.N researched data, contributed to discussion and reviewed/edited manuscript. A.B wrote the manuscript. We thank Meritxell Puig, Ángel Vázquez and Dr. Jesús Ruberte (UAB) for technical assistance. A.B is the guarantor of this work and, as such, had full access to all the data in the study and takes responsibility for the integrity of the data and the accuracy of the data analysis. This work was supported by the Fundació Marató TV3 (grant 201607.10) and 2017 SGR1468 to M.C. M.L.J, A.O and S.V are recipients of predoctoral fellowships from Generalitat de Catalunya (2019FI_B2 00061; 2020FI_B2 00037 and 2020FI_B1 00054, respectively). The authors declare that there is no conflict of interest.

APPENDIX A. SUPPLEMENTARY DATA

Supplementary data to this article can be found online at https://doi.org/10.1016/j.molmet.2021.101408.

DECLARATIONS OF INTEREST

None.

REFERENCES

[1] International Diabetes Federation, 2019. IDF diabetes atlas, 9th ed. Brussels, Belgium: International Diabetes Federation.

[2] Forbes, J.M., Cooper, M.E., 2013. Mechanisms of diabetic complications. Physiological Reviews 93(1):137–188.

[3] Pop-Busui, R., Boulton, A.J., Feldman, E.L., Bril, V., Freeman, R., Malik, R.A., et al., 2017. Diabetic neuropathy: a position statement by the American diabetes association. Diabetes Care 40(1):136–154.

[4] Pasnoor, M., Dimachkie, M.M., Kluding, P., Barohn, R.J., 2013. Diabetic neuropathy part 1: overview and symmetric phenotypes. Neurologic Clinics 31(2):425–445.

[5] Feldman, E.L., Callaghan, B.C., Pop-Busui, R., Zochodne, D.W., Wright, D.E., Bennett, D.L., et al., 2019. Diabetic neuropathy. Nature Reviews Disease Primers 5(1):41.

[6] Callaghan, B.C., Little, A.A., Feldman, E.L., Hughes, R.A., 2012. Enhanced glucose control for preventing and treating diabetic neuropathy. Cochrane Database of Systematic Reviews 6:CD007543.

[7] Callaghan, B.C., Gallagher, G., Fridman, V., Feldman, E.L., 2020. Diabetic neuropathy: what does the future hold? Diabetologia 63(5):891–897.

[8] Pande, M., Hur, J., Hong, Y., Backus, C., Hayes, J.M., Oh, S.S., et al., 2011. Transcriptional profiling of diabetic neuropathy in the BKS db/db mouse: a model of type 2 diabetes. Diabetes 60(7):1981–1989.

[9] Hinder, L.M., Vivekanandan-Giri, A., McLean, L.L., Pennathur, S., Feldman, E.L., 2013. Decreased glycolytic and tricarboxylic acid cycle intermediates coincide with peripheral nervous system oxidative stress in a murine model of type 2 diabetes. Journal of Endocrinology 216(1):1–11.

[10] Ma, J., Pan, P., Anyika, M., Blagg, B.S., Dobrowsky, R.T., 2015. Modulating molecular chaperones improves mitochondrial bioenergetics and decreases the inflammatory transcriptome in diabetic sensory neurons. ACS Chemical Neuroscience, 1637–1648.

[11] Hur, J., Dauch, J.R., Hinder, L.M., Hayes, J.M., Backus, C., Pennathur, S., et al., 2015. The metabolic syndrome and microvascular complications in a murine model of type 2 diabetes. Diabetes 64(9):3294–3304.

[12] O'Brien, P.D., Hur, J., Hayes, J.M., Backus, C., Sakowski, S.A., Feldman, E.L., 2015. BTBR ob/ob mice as a novel diabetic neuropathy model: neurological characterization and gene expression analyses. Neurobiology of Disease 73:348–355.

[13] Hur, J., Sullivan, K.A., Pande, M., Hong, Y., Sima, A.A., Jagadish, H.V., et al., 2011. The identification of gene expression profiles associated with progression of human diabetic neuropathy. Brain 134(Pt 11):3222–3235.

[14] Nie, L., Wu, G., Culley, D.E., Scholten, J.C., Zhang, W., 2007. Integrative analysis of transcriptomic and proteomic data: challenges, solutions and applications. Critical Reviews in Biotechnology 27(2):63–75.

[15] O'Brien, P.D., Sakowski, S.A., Feldman, E.L., 2014. Mouse models of diabetic neuropathy. ILAR Journal 54(3):259–272.

[16] Fan, B., Liu, X.S., Szalad, A., Wang, L., Zhang, R., Chopp, M., et al., 2018. Influence of sex on cognition and peripheral neurovascular function in diabetic mice. Frontiers in Neuroscience 12:795.

[17] Homs, J., Ariza, L., Pages, G., Verdu, E., Casals, L., Udina, E., et al., 2011. Comparative study of peripheral neuropathy and nerve regeneration in NOD and ICR diabetic mice. Journal of the Peripheral Nervous System 16(3):213–227.

[18] Vilches, J.J., Navarro, X., Verdú, E., 1995. Functional sudomotor responses to cholinergic agonists and antagonists in the mouse. Journal of the Autonomic Nervous System 55(1–2):105–111.

[19] Vilches, J.J., Wynick, D., Kofler, B., Lang, R., Navarro, X., 2012. Sudomotor function and sweat gland innervation in galanin knockout mice. Neuropeptides 46(4):151–155.

[20] Wiśniewski, J.R., Zougman, A., Nagaraj, N., Mann, M., 2009. Universal sample preparation method for proteome analysis. Nature Methods 6(5):359–362.

[21] Oliveros, J.C., 2007–2015. Venny. An interactive tool for comparing lists with Venn's diagrams.

[22] Liao, Y., Wang, J., Jaehnig, E.J., Shi, Z., Zhang, B., 2019. WebGestalt 2019: gene set analysis toolkit with revamped UIs and APIs. Nucleic Acids Research 47(W1):W199–W205.

[23] Huang, d.W., Sherman, B.T., Lempicki, R.A., 2009. Systematic and integrative analysis of large gene lists using DAVID bioinformatics resources. Nature Protocols 4(1):44—57.
[24] Szklarczyk, D., Gable, A.L., Lyon, D., Junge, A., Wyder, S., Huerta-Cepas, J., et al., 2019. STRING v11: protein-protein association networks with increased coverage, supporting functional discovery in genome-wide experimental datasets. Nucleic Acids Research 47(D1):D607—D613.
[25] Polpitiya, A.D., Qian, W.J., Jaitly, N., Petyuk, V.A., Adkins, J.N., Camp, D.G., et al., 2008. DAnTE: a statistical tool for quantitative analysis of -omics data. Bioinformatics 24(13):1556—1558.
[26] Robertson, D.M., Sima, A.A., 1980. Diabetic neuropathy in the mutant mouse [C57BL/ks(db/db)]: a morphometric study. Diabetes 29(1):60—67.
[27] Campero, M., Ezquer, M., Ezquer, F., 2015. Nerve excitability and structural changes in myelinated axons from diabetic mice. Experimental and Clinical Endocrinology & Diabetes 123(8):485—491.
[28] Kennedy, W.R., Navarro, X., 1989. Sympathetic sudomotor function in diabetic neuropathy. Archives of Neurology 46(11):1182—1186.
[29] Liu, Y., Sebastian, B., Liu, B., Zhang, Y., Fissel, J.A., Pan, B., et al., 2017. Sensory and autonomic function and structure in footpads of a diabetic mouse model. Scientific Reports 7:41401.
[30] Jo, S.H., Son, M.K., Koh, H.J., Lee, S.M., Song, I.H., Kim, Y.O., et al., 2001. Control of mitochondrial redox balance and cellular defense against oxidative damage by mitochondrial NADP+-dependent isocitrate dehydrogenase. Journal of Biological Chemistry 276(19):16168—16176.
[31] Schlattner, U., Tokarska-Schlattner, M., Wallimann, T., 2006. Mitochondrial creatine kinase in human health and disease. Biochimica et Biophysica Acta 1762(2):164—180.
[32] Maessen, D.E., Stehouwer, C.D., Schalkwijk, C.G., 2015. The role of methylglyoxal and the glyoxalase system in diabetes and other age-related diseases. Clinical Science 128(12):839—861.
[33] Horáková, L., Strosova, M.K., Spickett, C.M., Blaskovic, D., 2013. Impairment of calcium ATPases by high glucose and potential pharmacological protection. Free Radical Research 47(Suppl 1):81—92.
[34] Egnatchik, R.A., Leamy, A.K., Jacobson, D.A., Shiota, M., Young, J.D., 2014. ER calcium release promotes mitochondrial dysfunction and hepatic cell lipotoxicity in response to palmitate overload. Molecular Metabolism 3(5):544—553.
[35] Lupachyk, S., Watcho, P., Obrosov, A.A., Stavniichuk, R., Obrosova, I.G., 2013. Endoplasmic reticulum stress contributes to prediabetic peripheral neuropathy. Experimental Neurology 247:342—348.
[36] Padilla, A., Descorbeth, M., Almeyda, A.L., Payne, K., De Leon, M., 2011. Hyperglycemia magnifies Schwann cell dysfunction and cell death triggered by PA-induced lipotoxicity. Brain Research 1370:64—79.
[37] Sas, K.M., Kayampilly, P., Byun, J., Nair, V., Hinder, L.M., Hur, J., et al., 2016. Tissue-specific metabolic reprogramming drives nutrient flux in diabetic complications. JCI Insight 1(15):e86976.
[38] Cadenas, S., 2018. Mitochondrial uncoupling, ROS generation and cardioprotection. Biochimica et Biophysica Acta — Bioenergetics 1859(9):940—950.
[39] Maxson, M.E., Grinstein, S., 2014. The vacuolar-type H^+-ATPase at a glance - more than a proton pump. Journal of Cell Science 127(Pt 23):4987—4993.
[40] Akude, E., Zherebitskaya, E., Chowdhury, S.K., Smith, D.R., Dobrowsky, R.T., Fernyhough, P., 2011. Diminished superoxide generation is associated with respiratory chain dysfunction and changes in the mitochondrial proteome of sensory neurons from diabetic rats. Diabetes 60(1):288—297.
[41] Rojas, D.R., Kuner, R., Agarwal, N., 2019. Metabolomic signature of type 1 diabetes-induced sensory loss and nerve damage in diabetic neuropathy. Journal of Molecular Medicine (Berlin) 97(6):845—854.
[42] Ashford, A.J., Pain, V.M., 1986. Effect of diabetes on the rates of synthesis and degradation of ribosomes in rat muscle and liver in vivo. Journal of Biological Chemistry 261(9):4059—4065.
[43] Miller, M., Bower, E., Levitt, P., Li, D., Chantler, P.D., 1992. Myosin II distribution in neurons is consistent with a role in growth cone motility but not synaptic vesicle mobilization. Neuron 8(1):25—44.
[44] Roisen, F.J., Wilson, F.J., Yorke, G., Inczedy-Marcsek, M., Hirabayashi, T., 1983. Immunohistochemical localization of troponin-C in cultured neurons. Journal of Muscle Research & Cell Motility 4(2):163—175.
[45] Komori, N., Takemori, N., Kim, H.K., Singh, A., Hwang, S.H., Foreman, R.D., et al., 2007. Proteomics study of neuropathic and nonneuropathic dorsal root ganglia: altered protein regulation following segmental spinal nerve ligation injury. Physiol Genomics 29(2):215—230.
[46] McMillan, D.E., 1989. Increased levels of acute-phase serum proteins in diabetes. Metabolism 38(11):1042—1046.
[47] Hochepied, T., Berger, F.G., Baumann, H., Libert, C., 2003. Alpha(1)-acid glycoprotein: an acute phase protein with inflammatory and immunomodulating properties. Cytokine & Growth Factor Reviews 14(1):25—34.
[48] Lee, Y.S., Choi, J.W., Hwang, I., Lee, J.W., Lee, J.H., Kim, A.Y., et al., 2010. Adipocytokine orosomucoid integrates inflammatory and metabolic signals to preserve energy homeostasis by resolving immoderate inflammation. Journal of Biological Chemistry 285(29):22174—22185.
[49] Rosoklija, G.B., Dwork, A.J., Younger, D.S., Karlikaya, G., Latov, N., Hays, A.P., 2000. Local activation of the complement system in endoneurial microvessels of diabetic neuropathy. Acta Neuropathologica 99(1):55—62.
[50] de Jonge, R.R., van Schaik, I.N., Vreijling, J.P., Troost, D., Baas, F., 2004. Expression of complement components in the peripheral nervous system. Human Molecular Genetics 13(3):295—302.
[51] Camborieux, L., Bertrand, N., Swerts, J.P., 1998. Changes in expression and localization of hemopexin and its transcripts in injured nervous system: a comparison of central and peripheral tissues. Neuroscience 82(4):1039—1052.
[52] Lim, S.Y., Raftery, M.J., Goyette, J., Hsu, K., Geczy, C.L., 2009. Oxidative modifications of S100 proteins: functional regulation by redox. Journal of Leukocyte Biology 86(3):577—587.
[53] Leclerc, E., Fritz, G., Vetter, S.W., Heizmann, C.W., 2009. Binding of S100 proteins to RAGE: an update. Biochimica et Biophysica Acta 1793(6):993—1007.
[54] Jin, Y., Sharma, A., Carey, C., Hopkins, D., Wang, X., Robertson, D.G., et al., 2013. The expression of inflammatory genes is upregulated in peripheral blood of patients with type 1 diabetes. Diabetes Care 36(9):2794—2802.
[55] Zhou, Y., Rui, L., 2010. Major urinary protein regulation of chemical communication and nutrient metabolism. Vitamins & Hormones 83:151—163.
[56] Hui, X., Zhu, W., Wang, Y., Lam, K.S., Zhang, J., Wu, D., et al., 2009. Major urinary protein-1 increases energy expenditure and improves glucose intolerance through enhancing mitochondrial function in skeletal muscle of diabetic mice. Journal of Biological Chemistry 284(21):14050—14057.
[57] Zhou, Y., Jiang, L., Rui, L., 2009. Identification of MUP1 as a regulator for glucose and lipid metabolism in mice. Journal of Biological Chemistry 284(17):11152—11159.
[58] Baur, J.A., Pearson, K.J., Price, N.L., Jamieson, H.A., Lerin, C., Kalra, A., et al., 2006. Resveratrol improves health and survival of mice on a high-calorie diet. Nature 444(7117):337—342.
[59] Kleinert, M., Parker, B.L., Jensen, T.E., Raun, S.H., Pham, P., Han, X., et al., 2018. Quantitative proteomic characterization of cellular pathways associated with altered insulin sensitivity in skeletal muscle following high-fat diet feeding and exercise training. Scientific Reports 8(1):10723.
[60] Hinder, L.M., Murdock, B.J., Park, M., Bender, D.E., O'Brien, P.D., Rumora, A.E., et al., 2018. Transcriptional networks of progressive diabetic peripheral neuropathy in the db/db mouse model of type 2 diabetes: an inflammatory story. Experimental Neurology 305:33—43.

